Wang, Bin, de Godoi, Fernanda Condi, Sun, Zhiming, Zeng, Qingcong, Zheng, Shuilin, & Frost, Ray L.
(2015)
Synthesis, characterization and activity of an immobilized photocatalyst : natural porous diatomite supported titania nanoparticles.
Journal of Colloid and Interface Science, *438*, pp. 204-211.

Synthesis, characterization and activity of an immobilized photocatalyst: Natural porous diatomite supported TiO_2 nanoparticles

Bin Wang [a, b], Fernanda Condi de Godoi [b], Zhiming Sun [a], Qingcong Zeng [b], Shuilin Zheng [a,*], Ray L. Frost [c,**]

[a] *School of Chemical and Environmental Engineering, China University of Mining & Technology, Beijing 100083, PR China*

[b] *School of Chemistry and Molecular Biosciences, The University of Queensland, Brisbane Qld 4072, Australia*

[c] *Chemistry Discipline, Faculty of Science and Technology, Queensland University of Technology, Brisbane Qld 4001,Australia*

Email: b.wang6@uq.edu.au, f.condidegodoi@uq.edu.au, zhiming.baxia@163.com, qingcong.zeng@uq.net.au, shuilinzheng8@gmail.com, r.frost@qut.edu.au,

**Corresponding author. Fax: +86 10 62390972.*

***Corresponding author. Fax: +61 7 3138 2407.*

Abstract

Diatomite, a porous non-metal mineral, was used as support to prepare TiO_2/diatomite composites by a modified sol-gel method. The as-prepared composites were calcined at temperatures ranging from 450 to 950^oC. The characterization tests included X-ray powder diffraction (XRD), scanning electron microscopy (SEM) with an energy-dispersive X-ray spectrometer (EDS), High-resolution transmission electron microscopy (HRTEM), X-ray photoelectron spectroscopy (XPS), and nitrogen adsorption/desorption measurements. The XRD analysis indicated that the binary mixtures of anatase and rutile exist in the composites. The morphology analysis confirmed the TiO_2 particles were uniformly immobilized on the surface of diatom with a strong interfacial anchoring strength, which leads to few drain of photocatalytic components during practical applications. In further XPS studies of hybrid catalyst, we found the evidence of the presence of Ti—O—Si bond and increased percentage of surface hydroxyl. In addition, the adsorption capacity and photocatalytic activity of synthesized TiO_2/diatomite composites were evaluated by studying the degradation kinetics of aqueous Rhodamine B under UV-light irradiation. The photocatalytic degradation was found to follow pseudo-first order kinetics according to the Langmuir-Hinshelwood model. The preferable removal efficiency was observed in composites by 750^oC calcination, which is attributed to a relatively

appropriate anatase/rutile mixing ratio of 90/10.

Keywords: Diatomite; TiO_2; Adsorption; Photocatalysis

1. Introduction

Over the past decades, semiconductor photocatalysis attracted public interest as a promising technology for the removal of dye pollutants from textile and paper wastewater and of volatile organic compounds (VOCs) from indoor air [1, 2]. Semiconductor metal oxides, typically such as titanium dioxide (TiO_2), zinc oxide (ZnO), tin oxide (SnO_2), nickel oxide (NiO) and cuprous oxide (Cu_2O), have been used as photocatalysts [3-7]. Among them, TiO_2 is widely investigated because of its high photocatalytic activity, biological and chemical inertness, and non-toxic nature. However, from the standpoint of large-scale practical application and commercial benefits, TiO_2 nanoparticles (NPs) show disadvantages, which may result in a low photocatalytic efficiency and high cost. For example: strong tendency to aggregate, difficult to be recovered from the solution after treatment and low adsorption capacity. To overcome these drawbacks, recently many researchers are focused on immobilizing TiO_2 NPs on supports having large surface area and excellent adsorption capacity. This approach may enhance the TiO_2 NPs distribution in suspension which enables to adsorb and concentrate the target substances. Furthermore, the substances can easily diffuse from the adsorption site to the photocatalytic surface.

It has been demonstrated that heterogeneous photocatalytic reactions occurred on the surface of the catalyst and pre-adsorption of the target substrates around TiO_2 particles is critical for the degradation [1, 8]. Ao and Lu et al. [9, 10], for example, reported that TiO_2 immobilized onto the activated carbon shown a more effective photocatalytic activity for nitrogen oxide, BTEX (benzene, toluene, ethylbenzene and xylene) and formaldehyde. The strong adsorption of the pollutants over the activated

carbon was the main reason pointed by the authors to explain the occurred phenomenon. Recently, porous non-metal minerals have been taken into account as supports of TiO_2-based photocatalysts, such as perlite, zeolite and diatomite due to their low costs [11-14]. The use of porous minerals as support induces a synergistic effect by improving the photo-efficiency of the immobilized TiO_2 NPs. This effect can be associated to their high surface areas which avoid the formation of macroscopic aggregations of the photoactive particles.

Diatomite is a light fine-porous mineral consisting of extremely small diatom shells and its main chemical component is amorphous SiO_2. Diatomite has ordered pore-size distribution with specific properties such as high amorphous silica content, high porosity, and low density, which has been widely used in sound and heat insulation, as filters. Moreover, diatomite has outstanding merits as catalyst support for the removal of pollutants [15-18], from point of views of inert characteristics, substantial resources, practical use and environmental requirements [19]. The huge amount of silicon hydroxyl groups, acid sites and hydrogen bonds on the surface of amorphous SiO_2 can be considered as adsorption sites for pollutants [20-22]. Kou-Jong Hsien et al. [13] used three kinds of commercial anatase TiO_2 as photoactive particles supported in diatomite to study the photocatalytic efficiency of the bisphenol-A remediation. In our group, Sun et al. [14] evaluated the influence of the different support on the photocatalytic ability of TiO_2/amorphous silica minerals photocatalysts by using $TiCl_4$ as precursor through low-temperature hydrolysis-deposition method. . However, [14] only a few investigations have been reported about the effect of calcination temperature on the crystalline structure and photocatalytic performance of the TiO_2/diatomite photocatalysts prepared by sol-gel method. The synthetic method and calcination temperature may strongly affect the TiO_2 crystallinity, phase fraction and porous structure of the matrix, resulting a direct impact on the photocatalytic performance of catalysts [23].

Thus, in this study, a mixed phase TiO_2 immobilized on diatomite (TiO_2/diatomite) was successfully synthesized by a modified sol-gel method using tetrabutyl titanate (TBOT) as precursor. TiO_2 with different phase fraction and crystalline size was

found to exist in composites under different calcination temperatures. The photocatalytic performance of TiO_2/diatomite composites were evaluated by the degradation of dye Rhodamine B (RhB) in aqueous solution under UV light. The crystalline properties of TiO_2, porous structure of diatomite and the interface interaction were systematically characterized and studied.

2. Experimental

2.1. *Materials*

Raw diatomite (Linjiang, Jilin province, China) was used as catalyst support after purification. The process of purification was described in detail elsewhere [24]. The main chemical compositions of the purified diatomite (DE) are listed in **Table 1**. As summarized in **Table 1**, it is clear that the main chemical composition of porous diatomite mineral is amorphous SiO_2. Tetrabutyl titanate ($C_{16}H_{36}O_4Ti$, TBOT), ethanol (C_2H_5OH), hydrochloric acid (HCl), acetic acid (CH_3COOH), and Rhodamine B (RhB) were purchased from Beijing Reagent Co. (Beijing, China), which were all analytical reagent grade without any further purification before used. Pure commercial TiO_2 (Degussa P25) particles consists of 75% anatase and 25% rutile purchased from Degussa (Dusseldorf, Germany) was used for comparison purpose. Deionized water was used throughout all experimental procedures.

Table 1

Chemical constituent of purified diatomite (DE)

Constituent	SiO_2	Al_2O_3	Fe_2O_3	CaO	MgO	Na_2O	L.O.I.[a]
(%)	91.74	2.76	1.14	0.34	0.21	0.12	3.52

[a] Loss on ignition

2.2. *Preparation of TiO_2/diatomite composites*

The preparation of TiO_2/diatomite composites was undertaken by a modified sol-gel method as follows. Firstly, 1 g of DE dispersed in 14 mL of ethanol and 1 mL of acetic acid under stirring for 30min to form diatomite suspension. Secondly, 1.5 mL of TBOT were added dropwise into the diatomite suspension, under continuous

stirring, followed by the addition of 12 mL of ethanol: water solution (v:v=1:1; pH=2) which led the hydrolysis of the TBOT at moderate rate. After that, this solution was added dropwise into the suspension to arouse hydrolysis of TBOT at a moderate rate. The resulting mixture was stirred for 12 h to become aged and to immobilize as-synthesized TiO_2 colloids on the surface of DE. Finally, the product was dried in an oven at 105 ^oC for 4 h with subsequent calcination at 450~950 ^oC for 2 h in air at a heating rate of 2.5°/min. **Fig. 1** shows a schematic diagram of the possible pathways of Ti species [such as $Ti(OH)^{3+}$] deposited onto diatom in the synthesis process. In this study, the TiO_2/diatomite composites calcined at X ^oC were denoted as TD-X series listed in **Table 2**, respectively.

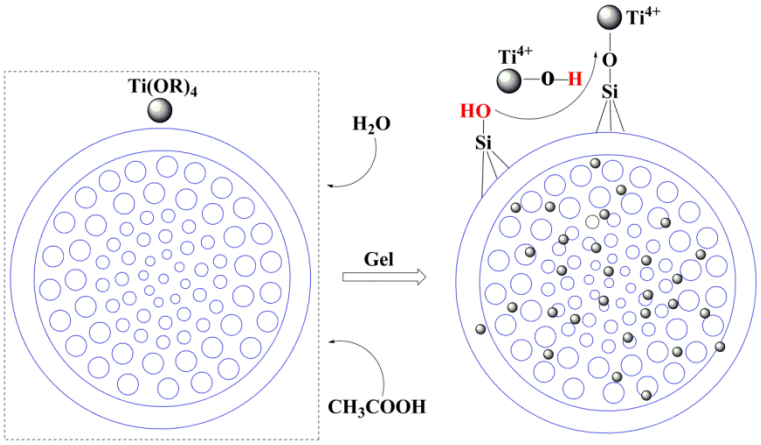

Fig.1 A schematic diagram of the possible pathways of Ti species [such as $Ti(OH)^{3+}$] deposited onto diatom.

2.3.*Characterization of TiO_2/diatomite composites*

The structures and crystal phases of TiO_2/diatomite composites were examined by X-ray powder diffraction (XRD) patterns with a Bruker D8 Advance X-ray diffractometer at 40 kV voltages and 20 mA current, using Cu Kα radiation at a scan rate of 4°/min. Phase content of TiO_2 was estimated from the strongest diffractions of anatase (101) and rutile (110), while the crystallite size (D) of TiO_2 was estimated by applying the Debye-Scherrer equation ($D = k\lambda / \beta \cos\theta$), where λ denotes the wavelength of the X-rays irradiation, k is usually taken as 0.89, and β is the corrected full width at half maxima (FWHM). The morphologies of samples were observed by scanning electron microscopy (SEM, EVO 18, Carl Zeiss) with an energy-dispersive X-ray spectrometer (EDS). High-resolution TEM (HRTEM) images and EDS

measurement were taken on a Philips Tecnai F20. The Brunauer-Emmett-Teller (BET) specific surface area of samples was determined at liquid-nitrogen temperature (77K) on a Micromeritcs ASAP 2020 system. The total pore volumes were calculated based on N_2 adsorption at a relative pressure of 0.99. Pore-size distributions were calculated from the adsorption branch of the isotherm, according to the Barrett-Joyner-Halenda (BJH) model [25]. In addition, X-ray photoelectron spectroscopy (XPS) was measured on a Kratos Axis Ultra spectrometer using Al Kα radiation (15 kV, 150 W). The survey spectra were recorded from 0 to 1200 eV at an energy interval of 1 eV/step. The C1s peak at 284.8 eV was used to calibrate the binding energies in XPS spectra.

2.4.*Adsorption and Photocatalysis of TiO_2/diatomite composites*

The adsorption and photocatalytic degradation of RhB were evaluated through a kinetic test. Aliquots were withdrawn from 100 ml of standard RhB aqueous solution (10 mg/L) containing 0.05 g of catalyst (P25 or as-prepared composites). Firstly, the suspensions were stirred in the dark for 1 hour to evaluate the adsorption performance. After establishing the equilibrium of adsorption, UV light irradiation was turned on. The photocatalytic reactions were carried out under UV-light irradiation afforded by a 250 W Hg lamp. All the collected samples of RhB solution were analyzed by UV-vis spectrophotometer (UV-9000S, Shanghai Yuanxi). The absorbance was measured at 562 nm. The percentage of RhB degradation (D_R) was calculated by the following equation:

$$D_R(\%) = \frac{C_0 - C_t}{C_0} \times 100\% \qquad \text{Eq. (1)}$$

where C_0 and C_t are concentrations of RhB before and after degradation, respectively.

3. Results and discussion

3.1 Crystalline phase studies

XRD technique was employed to analyze the crystalline phases of the diatomite support and TiO_2/diatomite composites calcined at different temperatures. The patterns, crystalline phase, fractional composition and crystallite size for different samples are shown in **Fig.2** and **Table 2**. In the patterns of raw diatomite, DE and TiO_2/diatomite catalysts calcined at relatively lower temperature, the broad peak centered at 2θ = 21.8° is assigned to the amorphous SiO_2 [18]. The diffraction line related to mineral impurities such as quartz and muscovite of the raw diatomite disappeared after purification. These impurities adhere to diatom and block pores (see SEM results), resulting a decrease in the surface area and adsorption capacity, which is harmful to concentrate dye molecules. When the calcination temperature applied is over 450°C, the diffraction peaks of anatase TiO_2 appear at 2θ = 25.4° (101), 37.9° (004) and 48.1° (200), which are consistent with the value in the standard card (JCPDS No. 21-1272). Further increase in calcination temperature (650-950°C) results in sharpening and narrowing of diffraction lines which corresponds to the enhancement in both degree of crystallinity and crystalline size. Moreover, when the calcination temperature reaches over 750°C, typical diffraction peaks corresponding to rutile TiO_2 (JCPDS No. 21-1276) appear in the XRD patterns of the TiO_2/diatomite composites. This transformation temperature is much higher than pristine TiO_2 (without mineral support) prepared by sol-gel method [26, 27]. It indicates that the presence of diatomite improves the thermal stability of the TiO_2 particles as a consequence of the enhanced distribution of TiO_2 NPs on the diatom surface. This result coincides with our early report about using $TiCl_4$ as precursor and low-temperature hydrolysis to prepare TiO_2/amorphous SiO_2 catalysts [14].

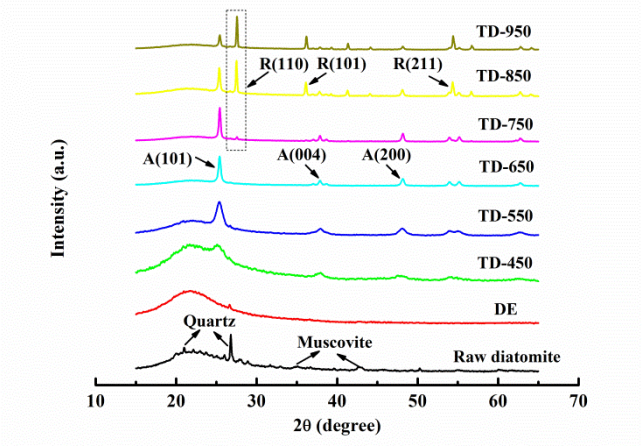

Fig.2 XRD patterns of diatomite and TiO_2/diatomite composites calcined at various temperatures.

Table 2

Summary of crystalline size calculated from XRD plots and surface characteristics of DE and TiO_2/diatomite composites calcined at various temperatures determined from N_2 physisorption at 77K.

Sample	Crystalline phase and size			Specific surface area, S_{BET} (m^2/g)	Pore volume, V_m (cm^3/g)	Average pore size, W (nm)
	Size of $A_{(101)}$ (nm)	Size of $R_{(110)}$ (nm)	Anatase ratio (%)			
DE	-	-	-	17.5	0.050	7.9
TD-450	8.3	-	-	34.5	0.079	5.3
TD-550	10.9	-	-	30.4	0.076	5.9
TD-650	17.7	-	100	15.3	0.049	7.7
TD-750	19.9	24.1	90.6	13.5	0.052	9.6
TD-850	29.4	46.0	36.6	6.5	0.028	11.5
TD-950	30.8	49.3	22.5	6.8	0.024	9.6

The crystalline sizes of anatase TiO_2 and rutile TiO_2 in samples were calculated using Debye-Scherrer equation. A common trend of increase in crystalline size both of anatase and rutile TiO_2 (see **Table 2**) occurs with the increase in calcination temperature for TiO_2/diatomite composites, due to high frequency of aggregation and sintering among the grains. In this study, the rutile content in the supported catalysts can be calculated based on the intensities of the peaks for anatase and rutile in the XRD patterns as follows [28, 29]:

$$X_R = \frac{I_R/I_A \times 0.79}{1 + I_R/I_A \times 0.79} \qquad \text{Eq. (2)}$$

where X_R is the weight fraction of the rutile phase in the supported catalysts, and I_A and I_R are the integrated X-ray intensities of the (101) reflection of anatase at 2θ = 25.4° and the (110) reflection of rutile at 2θ = 27.5°, respectively. The crystalline phase fractions are listed in **Table 2**. With the increasing of calcination temperature, the content of anatase phase decreases while the content of rutile phase increases. Based on the XRD results we can conclude that both crystalline size and phase fraction of TiO_2 immobilized on diatomite are depended on calcination temperature.

3.2 Morphology investigation

Fig.3 shows the surface morphology by SEM and TEM images of the raw diatomite, DE and TiO_2/diatomite composites calcined at different temperatures. The SEM images (**Fig.3a-c)** indicate that the diatom as the carrier exhibit highly porous disc-like shape with radius of *ca*. 30-40 μm. In **Fig. 3b** and **c**, after purification the surface of the diatom becomes clean and even, meanwhile regular pores are opened throughout with diameter around 50-100 nm. Moreover, the inherent pore structure of the diatom is relatively distinct for TD-750 (**Fig. 3d** and **e**), which may represent a benefit to adsorb pollutant molecules when it is used as the photocatalyst support [22]. In comparison to the clean surface of DE, the TiO_2/diatomite composites sample is obviously rougher, due to the deposition of TiO_2 particles on the diatom's surface. The ***Inset*** is related to the even distribution of titanium observed by the EDS mapping depicted for the TD-750 sample (**Fig. 3d**). **Fig. 3e** shows that the TiO_2 particles are preferentially gathered on the surrounding of pores rather than adhering on the surface of the diatom. Some pores are even covered by the TiO_2 particles. The high magnification SEM image of TD-950, **Fig. 3f,** illustrates the disc-like shape of the diatom destroyed by the high calcination temperature employed which resulted in serious aggregation of TiO_2 particles and sharp increase of average particle size according to the calculation result of XRD pattern.

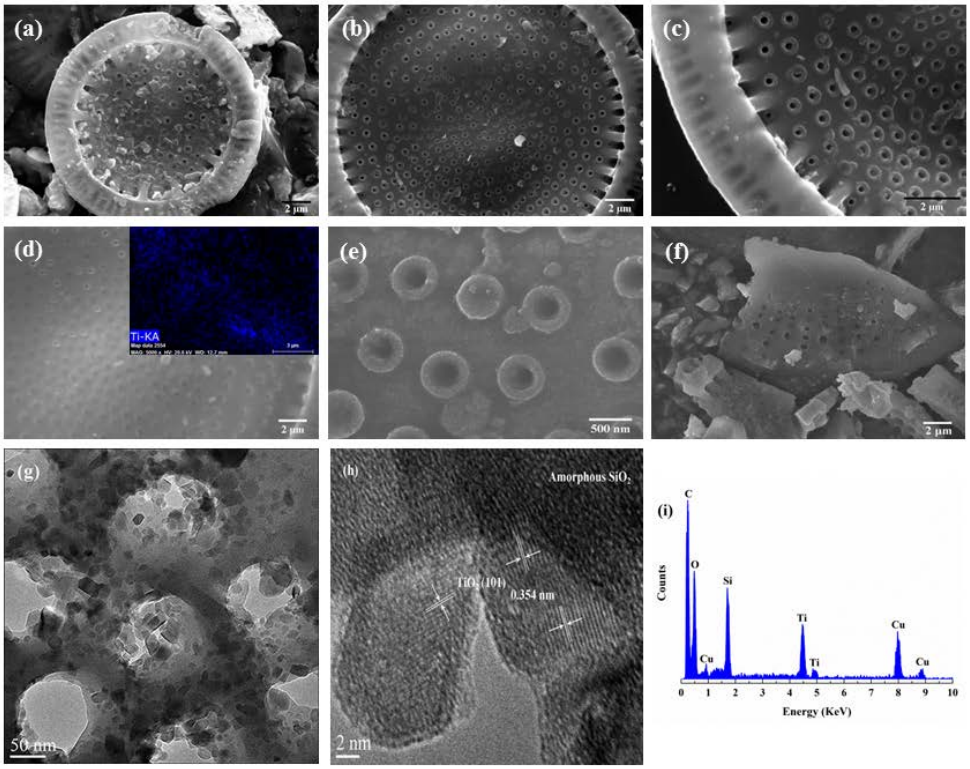

Fig.3 SEM images of (a) raw diatomite, (b-c) DE, (d-e) TD-750 with different magnifications and its Ti element surface distribution determined by EDS, (f) TD-950; and TEM image of (g) TD-750, (h-i) the corresponding HRTEM and EDS.

The morphology and composition of the TD-750 hybrid catalyst have been further investigated by TEM observations (**Fig. 3g** and **h**). It can be clearly found that these small TiO_2 NPs disperse very well. And the average particle size is *ca*. 15-30 nm, which is in good agreement with XRD calculated results.

This is also ascribed to the intimate interaction between bare TiO_2 NPs and diatom, which limits the crystalline TiO_2 NPs agglomeration to some extents. HRTEM image (**Fig. 3h**) of the product clearly shows the presence of lattice fringes hence indicating the crystalline nature of the TiO_2 and amorphous SiO_2. The spacing between the lattice fringes was measured to be around 0.354 nm which is in good agreement with the (101) planes of the anatase phase (0.352 nm) [30]. Moreover, the EDS measurement confirmed the composition of the hybrids (**Fig. 3i**), which demonstrated the presence of Si, Ti and O; meanwhile Cu signal is derived from the plated element for TEM measurement. Besides that, it is noteworthy that TiO_2

particles were still tightly anchored on the surface of diatom during the preparation of the TEM specimen even after a long time of mechanical stirring and sonication. From the TEM images, the presence of a strong interfacial anchoring strength between the TiO_2 NPs and the diatom can be confirmed, which leads to few drain of photocatalytic components during the practical applications. These results suggest that the TiO_2 NPs uniformly immobilized on the porous minerals matrix in the TiO_2/diatomite catalyst.

3.3 XPS studies

XPS was carried out to further analyze the chemical composition of the as-prepared TiO_2/diatomite hybrids. **Fig. 4a** depicts the survey spectra of the hybrids, TD-650, TD-750 and TD-850. The signals of O, Ti and Si elements can be clearly observed in the all samples. **Fig. 4b** reveals the high-resolution spectra for Ti 2p peaks. The spin-orbit components $2p_{3/2}$ and $2p_{1/2}$ of the Ti 2p peak could be deconvoluted by two peaks at approximately 459.4 and 465.3 eV, respectively (**Fig. 4b**). This indicates that the Ti elements mainly existed as Ti^{4+} [31, 32], and also confirmed by the difference in binding energy (BE) between the spin-orbit components of the Ti 2p peak which is close to 5.6 eV [33]. The shift observed on the Ti $2p_{3/2}$ peak position from *ca*. 458.2 eV (for pure TiO_2) to 459.4 eV (in presence of diatomite) might be related to higher electronegativity of Si in comparison to Ti [34]. It is suggested that the TiO_2 NPs are combined on the surface of diatom via Ti—O—Si bond [35, 36]. The deconvolutions of the O 1s peak of pristine TiO_2-750 and TD-750 shows three peaks in **Fig. 4c**. The peak of pure TiO_2 is assigned to titanium lattice (530.0 eV), the surface hydroxyl (531.8 eV) and adsorbed oxygen (533.1 eV) mainly from adsorbed water molecules [37, 38]. However, the peak intensity and position have changed in the spectrum of TD-750. The dominant peak at about 530.4 eV is still characteristic of TiO_2, and the peak at about 533.4 eV is corresponding to SiO_2 which is the main component of diatomite [35]. Additionally, the XPS shift of O 1s is another evidence of the presence of Ti—O—Si bond. According to the quantitative analysis (***Inset*** of

Fig. 4a), the atomic ratio of Ti is around 10%. It is very similar with the theoretic value resulting from the uniformly distribution of TiO_2 NPs on the diatomite's surface. The mole ratio of O and Ti plus Si for all samples was larger than 2. The calculated results indicated that the amount of the surface hydroxyl O increased notably in the TiO_2/diatomite composites (from 11.98% for the pristine TiO_2 to 20.40%). Several previous literatures have presented that the increase of the surface hydroxyl will lead to the enhancement of the photocatalytic efficiency [39, 40]. Therefore the increased percentage of surface hydroxyl on hybrid catalyst, resulting from the incorporation of diatomite matrix, will improve photocatalytic oxidation property.

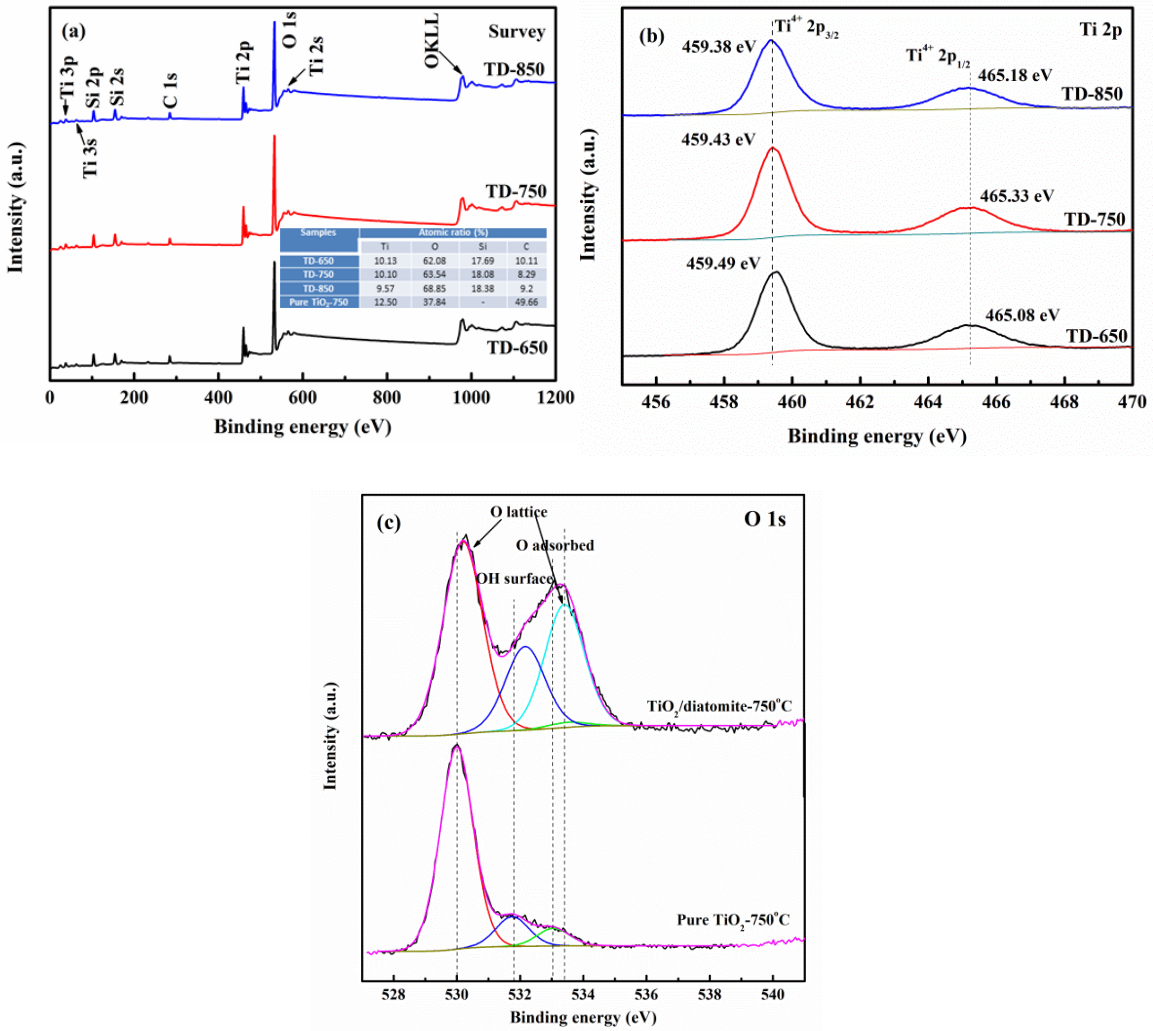

Samples	Atomic ratio (%)			
	Ti	O	Si	C
TD-650	10.13	62.08	17.69	10.11
TD-750	10.10	63.54	18.08	8.29
TD-850	9.57	68.85	18.38	9.2
Pure TiO_2-750	12.50	37.84	-	49.66

Fig.4 XPS spectra of pristine TiO_2-750°C and TiO_2/diatomite composites: (a) survey scan; (b) Ti 2p regions; and (c) deconvolution of O 1s. ***Inset*** is the relative contents of the elements in the sample.

3.4 Surface properties

Fig. 5 displays the nitrogen adsorption-desorption isotherms measured at 77K and the pore size distributions determined by the BJH method applied to the TiO_2/diatomite composites calcined at temperature ranging from 450 to 950^oC. The DE isotherm is used in terms of comparison. The nitrogen adsorption isotherms for all samples were classified as type IV according to the International Union of Pure and Applied Chemistry (IUPAC) [41]. As expected, the adsorption capacities of the composites decreased as the calcination temperature increased. At low relative pressure (P/P_0<0.4), samples TD-450 and TD-550 showed higher values of volume adsorbed per gram. This phenomenon was related to the predominance of smaller crystallite size species observed at lower calcination temperature condition (**Table 2**). At high relative pressure (P/P_0=0.4-0.98), the isotherms of TiO_2/diatomite composites calcined at 450-750^oC shows hysteresis behavior, reflecting a mesoporous structure. Furthermore, the pore size distribution of these samples show a narrower range of 5-10 nm than those of sample TD-850 and TD-950 (**Fig. 5b**). The result of DE shows a wider pore size distribution, which is in agreement with our previous study [18]. The pore structure parameters of the TiO_2/diatomite composites and DE, such as the specific surface area (S_{BET}), pore volume (V_m) and average pore size (W), are also summarized in **Table 2**. S_{BET} of TD-450 and TD-550 are higher than uncoated diatomite, which may be ascribed to low degree of crystallinity of TiO_2 phase on it. It should be also noted that the specific surface area of TiO_2/diatomite composites decreases with the increasing calcination temperature. When the calcination temperature increased to 850-950^oC, there is a sharp decrease, resulting from the partial microstructure destruction of support and aggregation of TiO_2 grains which blocked the pores of diatom (can be seen in **Fig. 3f**). Therefore, the pore structure parameters of the TiO_2/diatomite composites depend on the calcination temperature. And excess heating will lead to a destruction of disc-like diatom. Compared with uncoated diatomite, the little enhancement of pore volume for TD-750 is another proof to verify this modified sol-gel method we used can maintain the micro/mesopores of diatomite, which is benefit to the adsorption of contaminant molecules. This TiO_2/diatomite photocatalyst is credited to show an excellent

performance in future photocatalysis for aqueous and gaseous contaminants.

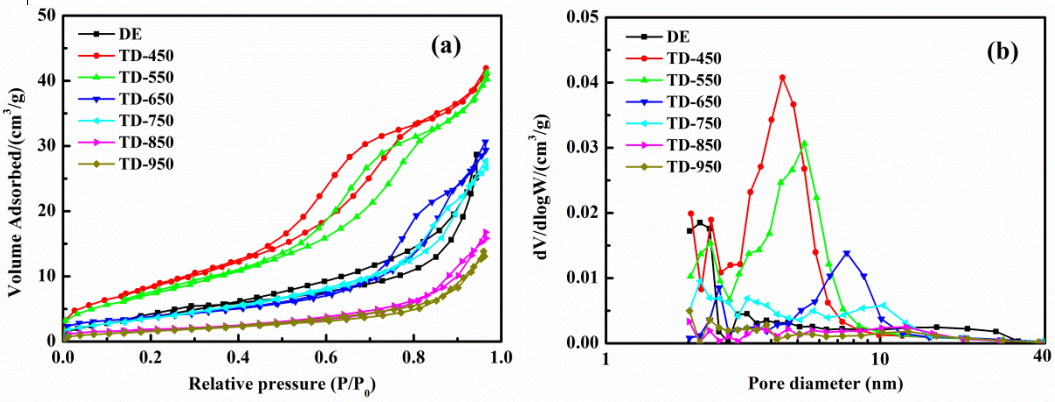

Fig.5 Nitrogen adsorption-desorption isotherms and (b) the corresponding pore size distributions of DE and TiO_2/diatomite composites calcined at various temperatures.

3.5 Adsorption and photocatalytic performance

We now turn to the main subject of this paper: the study of adsorption and UV-light derived photocatalysis behaviors of TiO_2/diatomite composites. The adsorption and photocatalytic curves are shown in **Fig. 6a**. Prior to UV light exposure, RhB uptake kinetics were performed using TD-450, TD-550, TD-750, TD-850, TD-650, TD-950, DE and P25 as sorbents (***inset*** of **Fig. 6a**). A fast adsorption rate is observed, it takes about 15 min to reach the equilibrium of adsorption-desorption for all samples. The mass balance equation (**Eq. 3**) was used to calculate the adsorption capacity of the sorbent for RhB at the equilibrium (t = 60 min), as summarized in **Table 3**.

$$Q_e = \frac{V(C_0 - C_e)}{M \times 1000} \qquad \text{Eq. (3)}$$

where C_0 and C_e are the initial and equilibrium concentrations of the RhB solution (mg/L), respectively, V is the volume of the RhB solution (mL), and M is the mass of sorbent (g). From **Table 3**, the adsorption capacity at equilibrium decreases in the following order: TD-450 > TD-550 > TD-750 > TD-650 > TD-850 > TD-950 > DE > P25. The higher adsorption capacities provided by the sorbents TD-450 and TD-550 may be related to their larger BET area and smaller TiO_2 particles (**Table 2**). Moreover, the hybrid composites express a better adsorption performance than DE,

because of the formation of active sites by the small TiO_2 particles [42, 43]. In comparison to TiO_2/diatomite composites, the adsorption capacity of pure TiO_2 nanoparticles (Degussa P25) is much lower. This behavior is assigned to the tendency of P25 particles aggregate in suspension [44]. The pore structure and large surface area of diatomite improves the distribution of as-prepared TiO_2 particles in suspension system. The favored adsorption of RhB molecule can accelerate the photooxidation of RhB in a synergetic way [44].

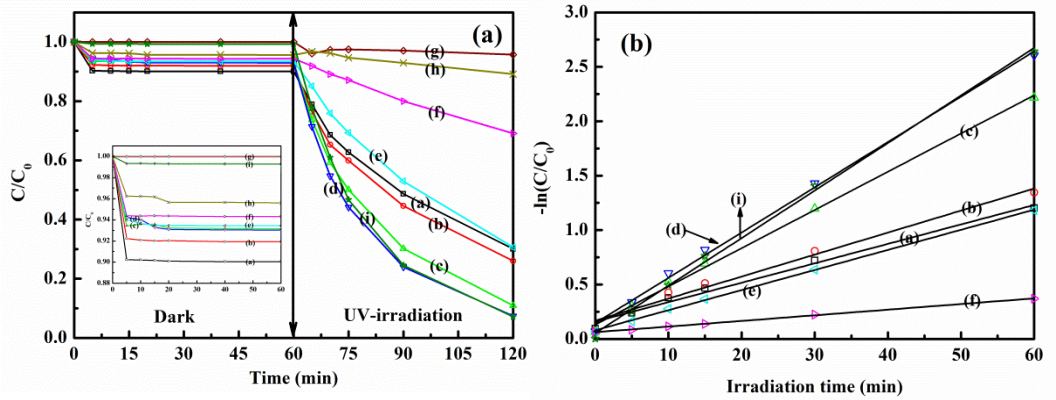

Fig.6 Adsorption and photocatalytic degradation kinetics of RhB under UV light irradiation for TiO_2/diatomite composites calcined at various temperatures: (a) 450°C, (b) 550°C, (c) 650°C, (d) 750°C, (e) 850°C, (f) 950°C. And for comparison, (g) Blank, (h) DE and (i) Degussa P25 were carried out.

Table 3: Results of adsorption and UV-light photocatalytic kinetic parameters over TiO_2/diatomite composites

Sample	Dark adsorption	UV-light-derived photocatalysis		
	Q_e (mg/g)	D_R (%)	k_{app} (min^{-1})	r^2
TD-450	0.67	70.0	0.018	0.98608
TD-550	0.54	73.7	0.020	0.98123
TD-650	0.46	89.1	0.035	0.99673
TD-750	0.48	92.6	0.042	0.99637
TD-850	0.44	69.4	0.018	0.99929
TD-950	0.38	30.9	0.0052	0.99891
Degussa P25	0.060	92.9	0.044	0.99771

The photocatalytic performance (**Fig. 6a**, UV-irradiation part) was evaluated by the percentage of RhB degradation (D_R), as expressed by **Eq. 1**. The results are described in **Table 3**. From the adsorption data, a better photocatalytic degradation performance was expected at 450°C and 550°C of calcination temperature. According to the literature [1, 8, 15], the adsorption can play an important role on the photocatalytic degradation reaction. However, in the present study, the

photodegradation performances greatly increase with the calcination temperature rise (from 450°C to 750°C), then dramatically decline at 850°C (see **Fig. 6a**, UV-irradiation part, and **Table 3**). This behavior is explained by the XRD results depicted in **Fig. 2**, based on the fact that both TiO_2 crystallinity and phase fraction are crucial to enhance the photocatalytic performance [45-47].

From **Fig. 2**, the anatase (101) peak starts to be well defined at 650°C. Samples TD-450 and TD-550 are characterized by the presence of TiO_2 in amorphous phase. The TD-750 sample shows the highest removal ratio (92.6%, from **Table 3**) with a mixing ratio of anatase/rutile of 90/10, respectively. The photodegradation decay at 850°C can be associated to the increase of rutile phase observed on the samples TD-850 and TD-950 (**Fig. 2**). The higher percentage of rutile phase and crystal particle dimension may inhibit the formation of ·OH radicals which slow down the reactants degradation [43]. Moreover, the microstructure has been fully destroyed at temperature higher than 750°C (**Fig. 3f**). Thus, it may be stated that a synergetic combination of the tuned adsorption conditions and TiO_2 crystalline structure is key parameter to improve the RhB photodegradation.

Fig. 6b depicts the photodegradation kinetics of RhB fitted by the pseudo-first order kinetic model, which could be explained in terms of Langmuir-Hinshelwood (LH) mechanism within the initial first hour [48]. The LH kinetic equation was mostly used to explain the heterogeneous catalytic process as given by:

$$r = -\frac{dC}{dt} = \frac{k_r K C}{1+KC} \qquad \text{Eq. (4)}$$

where r represents the rate of reaction that changes with time (t), k_r is the reaction rate constant and K is the adsorption rate constant. The rate expression based on LH expression can be deduced to first-order kinetics when t=0, C=C_0, it was described as follows:

$$-\ln\left(\frac{C}{C_0}\right) = k_{app}t \qquad \text{Eq. (5)}$$

where k_{app} represents the apparent rate constant, C represents the RhB concentration in aqueous solution at any time t during photocatalytic degradation, and t is reaction time. In this study, the apparent reaction rate constant (k_{app}) was used to compare the

photocatalytic activity of TiO_2/diatomite composites calcined at different temperatures. The summary of the photodegradation rate and the pseudo-first order kinetics of as-prepared composites under UV-light within 1h are shown in **Table 3**. The k_{app} increases in the order of TD-950 < TD-850 < TD-450 < TD-550 < TD-650 < TD-750, which is identical with the photodegradation results shown in **Fig. 6a**. All experiments demonstrated that the TiO_2 supported by diatomite possess a significant photocatalytic activity towards degrading the RhB dye in aqueous solution. Degussa P25 sample, which is composed by pure particles of TiO_2 showed D_R and k_{app} similar to the TD-750. However, the active material (TiO_2) content theoretically calculated to TD-750 is only 10 *wt*%.

Beside these, the disc-like composite photocatalyst assemblies are micron size which facilitates the solid-liquid separation in suspension (easy centrifugation and vacuum filtration). The results herein reported demonstrate that the composite TiO_2/diatomite is a promising candidate to be used as photocatalyst of RhB degradation in practice.

Conclusions

The TiO_2 NPs were successfully immobilized onto diatomite by a modified sol-gel method using tetrabutyl titanate as precursor. X-ray diffraction analysis displayed the influence of calcination temperature on TiO_2 crystallinity, phase fraction and TiO_2 crystalline size. In addition, SEM/TEM and EDS studies indicated a good distribution of TiO_2 particles on surface of disc-like diatom without blocking the pore of diatom. The presence of an interfacial anchoring strength between the TiO_2 NPs and diatom was confirmed by TEM results, which may inhibit the drain of photocatalytic components during the practical applications. Moreover, comparing the binding energies of Ti $2p_{3/2}$ and O 1s of TiO_2/diatomite composites with pristine TiO_2, it is concluded that the TiO_2 NPs is combined on the surface of diatomite through Ti—O—Si bond forming at the interface. And the increased percentage of surface hydroxyl on hybrid catalyst can improve photocatalytic oxidation property. The best experimental result for the photocatalytic degradation of dye RhB under UV-light was

found with TiO_2/diatomite composites calcination at 750^oC for 2 h having a 90/10 mixing ratio of anatase/rutile, which was confirmed by the photodegradation kinetics study and by the reaction rate constant of pseudo-first order kinetics calculated using the LH model. Therefore, we can conclude that in our case, the photocatalytic activities of TiO_2/diatomite composites are greatly dependent on the crystalline size and the anatase/rutile ratio rather than the BET surface area and the adsorption equilibrium amount of RhB. Namely, the calcination temperature is the crucial influence factor of catalyst photoactivity.

Acknowledgements

The authors gratefully acknowledge the financial support provided by National Technology R&D Program in the 12th five years plan of China (2011BAB03B07). The first author also thanks the China Scholarship Council (CSC) for financial support. And also the first author appreciates Professor Ian R. Gentle's suggestion and support, which make the first author be able to do experiment in School of Chemistry and Molecular Biosciences, The University of Queensland.

References

[1] J. Zhao, T. Wu, K. Wu, K. Oikawa, H. Hidaka, N. Serpone, Photoassisted Degradation of Dye Pollutants. 3. Degradation of the Cationic Dye Rhodamine B in Aqueous Anionic Surfactant/TiO_2 Dispersions under Visible Light Irradiation: Evidence for the Need of Substrate Adsorption on TiO_2 Particles, Environmental Science & Technology, 32 (1998) 2394-2400.

[2] C.H. Ao, S.C. Lee, Enhancement effect of TiO_2 immobilized on activated carbon filter for the photodegradation of pollutants at typical indoor air level, Applied Catalysis B: Environmental, 44 (2003) 191-205.

[3] X. Chen, Titanium Dioxide Nanomaterials: Synthesis, Properties, Modifications, and Applications, Chemical reviews, 107 (2007) 2891-2959.

[4] F. Lu, W. Cai, Y. Zhang, ZnO Hierarchical Micro/Nanoarchitectures: Solvothermal Synthesis and Structurally Enhanced Photocatalytic Performance, Advanced Functional Materials, 18 (2008) 1047-1056.

[5] L. Shi, H. Lin, Facile Fabrication and Optical Property of Hollow SnO_2 Spheres and Their Application in Water Treatment, Langmuir, 26 (2010) 18718-18722.

[6] B. Zhao, X.-K. Ke, J.-H. Bao, C.-L. Wang, L. Dong, Y.-W. Chen, H.-L. Chen, Synthesis of Flower-Like NiO and Effects of Morphology on Its Catalytic Properties, The Journal of Physical Chemistry C, 113 (2009) 14440-14447.

[7] J. Kondo, Cu_2O as a photocatalyst for overall water splitting under visible light irradiation,

Chemical Communications, (1998) 357-358.
[8] Q. Wang, C. Chen, D. Zhao, W. Ma, J. Zhao, Change of Adsorption Modes of Dyes on Fluorinated TiO_2 and Its Effect on Photocatalytic Degradation of Dyes under Visible Irradiation, Langmuir, 24 (2008) 7338-7345.
[9] C.H. Ao, S.C. Lee, Combination effect of activated carbon with TiO_2 for the photodegradation of binary pollutants at typical indoor air level, Journal of Photochemistry and Photobiology A: Chemistry, 161 (2004) 131-140.
[10] Y. Lu, D. Wang, C. Ma, H. Yang, The effect of activated carbon adsorption on the photocatalytic removal of formaldehyde, Building and Environment, 45 (2010) 615-621.
[11] S.N. Hosseini, S.M. Borghei, M. Vossoughi, N. Taghavinia, Immobilization of TiO_2 on perlite granules for photocatalytic degradation of phenol, Applied Catalysis B: Environmental, 74 (2007) 53-62.
[12] V. Durgakumari, M. Subrahmanyam, K.V. Subba Rao, A. Ratnamala, M. Noorjahan, K. Tanaka, An easy and efficient use of TiO_2 supported HZSM-5 and TiO_2+HZSM-5 zeolite combinate in the photodegradation of aqueous phenol and p-chlorophenol, Applied Catalysis A: General, 234 (2002) 155-165.
[13] K.-J. Hsien, W.-T. Tsai, T.-Y. Su, Preparation of diatomite–TiO_2 composite for photodegradation of bisphenol-A in water, J Sol-Gel Sci Technol, 51 (2009) 63-69.
[14] Z. Sun, C. Bai, S. Zheng, X. Yang, R.L. Frost, A comparative study of different porous amorphous silica minerals supported TiO_2 catalysts, Applied Catalysis A: General, 458 (2013) 103-110.
[15] Y. Jia, W. Han, G. Xiong, W. Yang, Layer-by-layer assembly of TiO_2 colloids onto diatomite to build hierarchical porous materials, Journal of Colloid and Interface Science, 323 (2008) 326-331.
[16] D. Liu, W. Yuan, P. Yuan, W. Yu, D. Tan, H. Liu, H. He, Physical activation of diatomite-templated carbons and its effect on the adsorption of methylene blue (MB), Applied Surface Science, 282 (2013) 838-843.
[17] L. Zhou, W. Song, Z. Chen, G. Yin, Degradation of Organic Pollutants in Wastewater by Bicarbonate-Activated Hydrogen Peroxide with a Supported Cobalt Catalyst, Environmental Science & Technology, 47 (2013) 3833-3839.
[18] Z. Sun, S. Zheng, G.A. Ayoko, R.L. Frost, Y. Xi, Degradation of simazine from aqueous solutions by diatomite-supported nanosized zero-valent iron composite materials, Journal of Hazardous Materials, 263, Part 2 (2013) 768-777.
[19] S.É. Ivanov, A.V. Belyakov, Diatomite and its applications, Glass Ceram, 65 (2008) 48-51.
[20] P. Yuan, D.Q. Wu, H.P. He, Z.Y. Lin, The hydroxyl species and acid sites on diatomite surface: a combined IR and Raman study, Applied Surface Science, 227 (2004) 30-39.
[21] J. Yuan, M. Chen, J. Shi, W. Shangguan, Preparations and photocatalytic hydrogen evolution of N-doped TiO_2 from urea and titanium tetrachloride, International Journal of Hydrogen Energy, 31 (2006) 1326-1331.
[22] N. An, W. Zhang, X. Yuan, B. Pan, G. Liu, M. Jia, W. Yan, W. Zhang, Catalytic oxidation of formaldehyde over different silica supported platinum catalysts, Chemical Engineering Journal, 215–216 (2013) 1-6.
[23] H. Khan, D. Berk, Sol–gel synthesized vanadium doped TiO_2 photocatalyst: physicochemical properties and visible light photocatalytic studies, J Sol-Gel Sci Technol, 68 (2013) 180-192.
[24] Z. Sun, X. Yang, G. Zhang, S. Zheng, R.L. Frost, A novel method for purification of low grade diatomite powders in centrifugal fields, International Journal of Mineral Processing, 125 (2013) 18-26.

[25] J.C. Yu, J. Yu, J. Zhao, Enhanced photocatalytic activity of mesoporous and ordinary TiO_2 thin films by sulfuric acid treatment, Applied Catalysis B: Environmental, 36 (2002) 31-43.
[26] K. Farhadian Azizi, M.M. Bagheri-Mohagheghi, Transition from anatase to rutile phase in titanium dioxide (TiO_2) nanoparticles synthesized by complexing sol–gel process: effect of kind of complexing agent and calcinating temperature, J Sol-Gel Sci Technol, 65 (2013) 329-335.
[27] N.R.C. Fernandes Machado, V.S. Santana, Influence of thermal treatment on the structure and photocatalytic activity of TiO_2 P25, Catalysis Today, 107–108 (2005) 595-601.
[28] A.H. Chan, J.F. Porter, J.P. Barford, C.K. Chan, Effect of thermal treatment on the photocatalytic activity of TiO_2 coatings for photocatalytic oxidation of benzoic acid, Journal of Materials Research, 17 (2002) 1758-1765.
[29] G. Colon, J. Sanchez-Espana, M. Hidalgo, J. Navío, Effect of TiO_2 acidic pre-treatment on the photocatalytic properties for phenol degradation, Journal of Photochemistry and Photobiology A: Chemistry, 179 (2006) 20-27.
[30] R. Jaiswal, N. Patel, D.C. Kothari, A. Miotello, Improved visible light photocatalytic activity of TiO_2 co-doped with Vanadium and Nitrogen, Applied Catalysis B: Environmental, 126 (2012) 47-54.
[31] B.M. Reddy, P.M. Sreekanth, Y. Yamada, Q. Xu, T. Kobayashi, Surface characterization of sulfate, molybdate, and tungstate promoted TiO_2-ZrO_2 solid acid catalysts by XPS and other techniques, Applied Catalysis A: General, 228 (2002) 269-278.
[32] T. Yu, X. Tan, L. Zhao, Y. Yin, P. Chen, J. Wei, Characterization, activity and kinetics of a visible light driven photocatalyst: Cerium and nitrogen co-doped TiO_2 nanoparticles, Chemical Engineering Journal, 157 (2010) 86-92.
[33] N. Rajkumar, K. Ramachandran, Oxygen Deficiency and Room Temperature Ferromagnetism in Undoped and Cobalt-Doped TiO_2 Nanoparticles, Nanotechnology, IEEE Transactions on, 10 (2011) 513-519.
[34] Y.-L. Lin, T.-J. Wang, Y. Jin, Surface characteristics of hydrous silica-coated TiO_2 particles, Powder Technology, 123 (2002) 194-198.
[35] T. Lopez, P. Bosch, F. Tzompantzi, R. Gomez, J. Navarrete, E. Lopez-Salinas, M. Llanos, Effect of sulfation methods on TiO_2–SiO_2 sol–gel catalyst acidity, Applied Catalysis A: General, 197 (2000) 107-117.
[36] Y.-h. Xu, Z.-x. Zeng, The preparation, characterization, and photocatalytic activities of Ce-TiO_2/SiO_2, Journal of Molecular Catalysis A: Chemical, 279 (2008) 77-81.
[37] G. Li, C. Liu, Y. Liu, Different effects of cerium ions doping on properties of anatase and rutile TiO_2, Applied Surface Science, 253 (2006) 2481-2486.
[38] Z. Liu, B. Guo, L. Hong, H. Jiang, Preparation and characterization of cerium oxide doped TiO_2 nanoparticles, Journal of Physics and Chemistry of Solids, 66 (2005) 161-167.
[39] Y. Nosaka, S. Komori, K. Yawata, T. Hirakawa, A.Y. Nosaka, Photocatalytic OH radical formation in TiO_2 aqueous suspension studied by several detection methods, Physical Chemistry Chemical Physics, 5 (2003) 4731-4735.
[40] L. Li, C.-y. Liu, Y. Liu, Study on activities of vanadium (IV/V) doped TiO_2(R) nanorods induced by UV and visible light, Materials Chemistry and Physics, 113 (2009) 551-557.
[41] R. Pierotti, J. Rouquerol, Reporting physisorption data for gas/solid systems with special reference to the determination of surface area and porosity, Pure and Applied Chemistry, 57 (1985) 603-619.
[42] K. Lv, J. Yu, K. Deng, J. Sun, Y. Zhao, D. Du, M. Li, Synergistic effects of hollow structure and surface fluorination on the photocatalytic activity of titania, Journal of Hazardous Materials, 173 (2010)

539-543.
[43] C.G. Silva, J.L. Faria, Effect of key operational parameters on the photocatalytic oxidation of phenol by nanocrystalline sol–gel TiO_2 under UV irradiation, Journal of Molecular Catalysis A: Chemical, 305 (2009) 147-154.
[44] C.-T. Hsieh, W.-S. Fan, W.-Y. Chen, J.-Y. Lin, Adsorption and visible-light-derived photocatalytic kinetics of organic dye on Co-doped titania nanotubes prepared by hydrothermal synthesis, Separation and Purification Technology, 67 (2009) 312-318.
[45] B. Ohtani, S. Nishimoto, Effect of surface adsorptions of aliphatic alcohols and silver ion on the photocatalytic activity of titania suspended in aqueous solutions, The Journal of Physical Chemistry, 97 (1993) 920-926.
[46] G. Tian, H. Fu, L. Jing, B. Xin, K. Pan, Preparation and Characterization of Stable Biphase TiO_2 Photocatalyst with High Crystallinity, Large Surface Area, and Enhanced Photoactivity, The Journal of Physical Chemistry C, 112 (2008) 3083-3089.
[47] K.-J. Hwang, J.-W. Lee, W.-G. Shim, H.D. Jang, S.-I. Lee, S.-J. Yoo, Adsorption and photocatalysis of nanocrystalline TiO_2 particles prepared by sol–gel method for methylene blue degradation, Advanced Powder Technology, 23 (2012) 414-418.
[48] Y. Li, S. Sun, M. Ma, Y. Ouyang, W. Yan, Kinetic study and model of the photocatalytic degradation of rhodamine B (RhB) by a TiO_2-coated activated carbon catalyst: Effects of initial RhB content, light intensity and TiO_2 content in the catalyst, Chemical Engineering Journal, 142 (2008) 147-155.

Figure captions:

Fig.1 A schematic diagram of the possible pathways of Ti species [such as $Ti(OH)^{3+}$] deposited onto diatom.

Fig.2 XRD patterns of diatomite and TiO_2/diatomite composites calcined at various temperatures.

Fig.3 SEM images of (a) raw diatomite, (b-c) DE, (d-e) TD-750 with different magnifications and its Ti element surface distribution determined by EDS, (f) TD-950; and TEM image of (g) TD-750, (h-i) the corresponding HRTEM and EDS.

Fig.4 XPS spectra of pristine TiO_2-750^oC and TiO_2/diatomite composites: (a) survey scan; (b) Ti 2p regions; and (c) deconvolution of O 1s. ***Inset*** is the relative contents of the elements in the sample.

Fig.5 (a) Nitrogen adsorption-desorption isotherms and (b) the corresponding pore size distributions of DE and TiO_2/diatomite composites calcined at various temperatures.

Fig.6 Adsorption and photocatalytic degradation kinetics of RhB under UV light irradiation for TiO_2/diatomite composites calcined at various temperatures: (a) 450^oC, (b) 550^oC, (c) 650^oC, (d) 750^oC, (e) 850^oC, (f) 950^oC. And for comparison, (g) Blank, (h) DE and (i) Degussa P25 were carried out.